Applied Catalysis B: Environmental 132–133 (2013) 195–203

Contents lists available at SciVerse ScienceDirect

Applied Catalysis B: Environmental

journal homepage: www.elsevier.com/locate/apcatb

Reaction kinetics investigation of the selective oxidation of aqueous ethanol solutions with air over a Au/TiO_2 catalyst

Pedram Aghaei [a], Rob J. Berger [b,*]

[a] Laboratory of Industrial Chemistry, Ruhr-University Bochum, D-44780 Bochum, Germany
[b] Anaproc c/o Delft University of Technology, Julianalaan 136, 2628 BL Delft, The Netherlands

ARTICLE INFO

Article history:
Received 29 August 2012
Received in revised form
20 November 2012
Accepted 23 November 2012
Available online 1 December 2012

Keywords:
Aerobic oxidation of aqueous ethanol
Gold catalysts
Production of acetic acid
Reaction kinetics

ABSTRACT

The selective oxidation of aqueous ethanol solution with air over a powdered commercial 1 wt% Au/TiO_2 catalyst was investigated in stirred mini-autoclaves. The catalyst was characterized by various techniques including N_2 physisorption, XRD, ICP-OES, and TEM. Temperature, pressure, initial ethanol concentration, catalyst concentration, and reaction time were varied in order to successfully determine the parameters of a Langmuir–Hinshelwood–Hougen–Watson type reaction kinetics model, which was derived from the surface reactions. It is assumed that hydrogen abstraction by surface hydroxyl species is the rate-determining step. The model adequately describes the decreasing conversion at higher ethanol concentration and also the selectivities towards the products acetaldehyde, acetic acid, ethyl acetate, and CO_2. The moderate description of the conversion at 180–200 °C can be improved by expanding the model with a second reaction route.

1. Introduction

The selective oxidation of primary alcohols in aqueous phase by use of molecular oxygen or hydrogen peroxide to their respective aldehydes or ketones is considered an important, commercially applied process route in the synthesis of fine chemicals [1–6]. The oxidation of alcohols has been traditionally based on the use of stoichiometric amounts of oxidants, i.e. chromate or permanganate, which makes the catalytic reaction expensive and also from environmentally point of view unattractive [1,7–9]. Different heterogeneous and homogeneous catalysts have been investigated for this reaction to find alternative methods which should be both economically efficient and environmentally benign [10–13]. The homogeneous catalysts applied on industrial scale suffer from several problems related with corrosion and plating out on the reactor wall, handling, recovery, and reuse of the catalyst [13]. Heterogeneous catalysts seem to be more promising catalysts due to the ease of recovery and reuse. A variety of heterogeneous catalytic systems with gold-based catalysts that are able to oxidize primary alcohols have been intensively investigated [2,14–19] mainly due to their high chemoselectivity [17].

For many years metallic gold was considered too inactive to be useful as a catalyst [20]. The remarkable catalytic behavior shown by gold depends on forming it into very small particles (<10 nm) due to the inability of the large particles to chemisorb typical reactant molecules to any useful extent [21,22]. Metal oxide-supported gold catalysts are well known for their high activity in the low temperature oxidation of CO with potential applications in fuel cells [23,24]. Key factors affecting the high activity of the catalyst are the oxidation state of the active cationic Au species [25,26], the strong influence of the Au nanoparticles size [21,27–30], and also the active sites at the interface between the Au nanoparticles and metal oxide support [31–35].

Herein, as a step in the investigation of the applicability of active supported gold catalysts for the selective oxidation of aqueous ethanol to acetic acid, the reaction kinetics on a commercially available Au/TiO_2 catalyst has been determined. According to our best knowledge, this is the first thorough kinetic investigation on the aerobic oxidation of aqueous ethanol solution using a gold catalyst. A commercial 1 wt% Au/TiO_2 catalyst has been chosen for this study because of its high catalytic activity and yields toward acetic acid in the absence of solvent and base among other supported noble metal catalysts in the oxidation of primary alcohols [15–17]. Knowledge of the reaction kinetics is very useful to find the optimal process conditions and also to determine the sensitivity of the catalyst performance on the reaction conditions for a proper process design, which will be economically and environmentally efficient. To determine the reaction kinetics, the relevant process conditions were varied, such as temperature, pressure, catalyst concentration, initial ethanol concentration, reaction time, and stirring rate.

* Corresponding author. Tel.: +31 0 15 2784316; fax: +31 0 15 2785006.
E-mail address: R.J.Berger@tudelft.nl (R.J. Berger).
URL: http://www.anaproc.com/ (R.J. Berger).

0926-3373/$ – see front matter © 2012 Elsevier B.V. All rights reserved.
http://dx.doi.org/10.1016/j.apcatb.2012.11.039

2. Experimental

2.1. Catalyst and chemicals

The commercially available AURO*lite*™ gold catalyst consisting of 1 wt% Au/TiO_2 (AUROlite™, Strem 79-0165 in collaboration with Project AuTEK) [36] was used in this investigation. Before testing, the catalyst was crushed for several minutes to obtain particles of about 10 μm and smaller determined by using a light microscope. Ethanol (ethanol absolute) was obtained from Sigma-Adrich, and water (HPLC Gradient Grade) was supplied by J.T. Baker. To dilute the reaction mixture, acetone (J.T. Baker) was used as a solvent. Synthetic air obtained from *AIR LIQUIDE* consisting of 20.5% O_2 in N_2 was used to pressurize the reactors.

2.2. Catalyst characterization

Elemental analysis of the catalyst was performed using ICP optical emission spectroscopy (ICP–OES) with an UNICAM 701 spectrometer from UNICAM. The textural properties of the catalyst were determined via N_2 physisorption at −196 °C using a NOVA 2000 series setup supplied by Quantachrome. Each sample was degassed under vacuum at 200 °C for 2 h. Transmission electron microscopy (TEM) images of the catalyst were recorded using a Hitachi H-8100 electron microscope equipped with a LaB_6 filament and operated at 200 kV. The catalyst samples were prepared by placing a droplet of the powder material dispersed in 2-propanol on a carbon-coated-mesh Au grid. XRD measurements were carried out with a Panalytical MPD Bragg–Brentano θ–θ diffractometer equipped with CuK_α radiation (40 kV and 40 mA).

2.3. Kinetic experiments

The kinetic experiments were carried out by using a multiple reactor system (Parr Series 5000) manufactured by Parr Instrument Company. The reaction unit includes six 75 ml high pressure stainless steel reaction vessels operating in parallel. Each reaction vessel is equipped with inlet and exhaust valves, pressure transducer in addition to an internal J-type thermocouple located inside a thermowell in direct contact with the liquid. The cylindrical reaction vessels were supplied with well-fitting glass liners to avoid direct contact of the reaction mixture with the steel wall (Fig. 1). The internal diameter, internal height, and thickness of the wall of the glass liners were 38, 55, and 2.0 mm, respectively.

All six vessels were stirred at 350 rpm (standard condition) with a magnetic stirrer system by flea micro magnetic stirring bars (Teflon PTFE coated) with a length of 22 mm and a diameter of 5 mm. A stirring rate of 350 rpm was sufficient to distribute the catalyst homogeneously in the entire liquid volume. This was supported by close visual examination by checking the mixing in the same glass container outside the steel housing, showing a homogeneous mixing of the catalyst throughout the liquid and absence of any stagnant zones. Additionally, the assumption of a homogeneous distribution was supported by experimental results in which the stirring rate was varied and an increase of the stirring rate to 500 rpm did not appreciably influence the results, whereas a decrease to 200 rpm showed a small but significant decrease in conversion. This mixing rate also achieved absence of significant transport limitation of oxygen from the head space into the liquid. This was verified by calculating the mass transfer limitation using a typical mass transfer rate k_La in a small well-mixed magnetic flea laboratory vessel of 0.1 s^{-1} (k_L is the mass transfer coefficient expressed in $m^3\,m^{-2}\,s^{-1}$ and a is the gas-liquid interfacial area expressed in $m^2\,m^{-3}$), which is still below 5% in the experiment with the highest reaction rate used, yielding a conversion of 91%.

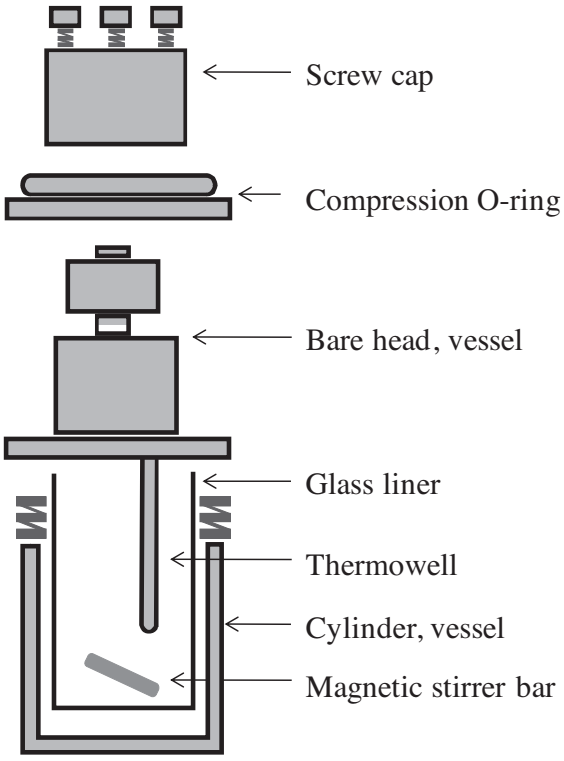

Fig. 1. Schematic representation of the reactor configuration.

Temperature, pressure, and stirring speed were recorded continuously for each reactor separately on a PC. 10 mL of the reaction mixture (5 wt% ethanol in water, unless otherwise specified) was filled into the reaction vessels in addition to 100 mg (unless otherwise specified) of the gold catalyst. The remaining gas volume is 90 mL of which 65 mL in the reactor vessel above the liquid and 25 mL in the dead space between the valve and the reactor. After pressurizing with synthetic air to 30 bar (unless otherwise specified), the reactors were heated under stirring in about 50 min to reach required reaction temperature. The reactors were kept at the reaction temperature during the predetermined reaction time (4 hours, unless otherwise specified), followed by about 40 min cooling to 70 °C and then using an ice bath to below 5 °C. After depressurization, the reaction mixture was collected and filtrated to obtain a catalyst-free liquid mixture. The composition of the reaction products in the liquid phase was determined by a gas chromatography-mass spectrometry (GC-MS) using a Shimadzu GC-MS QP 2010 plus instrument. External standard calibration was applied, since the instrument was supplied with an automatic sampler able to inject always exactly the same volume of liquid. The instrument separated the liquid components using a SGE BPX-5 capillary column with dimensions of 30 m × 0.25 mm × 0.25 μm. Ultra-pure helium gas (99.999% He) was used as carrier gas with flow rate of 97.6 ml min^{-1}. The temperature program used for sample analysis was the following: the oven was set at 45 °C for 3 min, then the temperature increased at a rate of 25 °C min^{-1} up to 200 °C and remained constant for 4 min. The detector temperature was 250 °C. MS spectra were compared with the spectra gathered in the NIST library program with a fit higher than 90%.

The effect of deactivation of the catalyst was minimized by using a fresh sample of the catalyst for each experiment. This is important since Jørgensen et al. [17] reported a significant deactivation of the Au/TiO_2 catalyst upon reuse of the catalyst, although the catalyst remained active even after several runs. For the Au/$MgAl_2O_4$ catalyst they observed a similar rate of deactivation. However, they did not observe a significant coking of the catalyst.

The conversion of ethanol was calculated with Eq. (1) and the selectivities of the products were calculated with Eq. (2), with the stoichiometric number, ν_i, being 2 for ethyl acetate and 1 for the other products.

$$X_A = \frac{N_{A,0} - N_A}{N_{A,0}} \quad (1)$$

$$S_i = \frac{\nu_i N_i}{N_{A,0} - N_A} \quad (2)$$

where X_A = conversion of reactant A [–]; $N_{A,0}$ = initial amount of reactant A [mol]; N_A = final amount of reactant A [mol]; ν_i = stoichiometric number of product i [–]; N_i = amount of product i formed [mol]; S_i = selectivity of product i [–].

Since the selectivities do not sum up to unity and CO_2 has been identified as a major byproduct in this reaction on comparable catalysts [16,17], it was assumed that the only remainder was CO_2. Unfortunately, this results in a large scatter in the CO_2 selectivity, because it comprises the inaccuracies of the analysis of all the other components.

It is noted that there was typically a few percent loss of the reactants and products due to evaporation during handling, i.e. preparing the reaction mixtures, filtration of the final mixture, and preparation of the samples for analysis. The results were corrected for this using the average deviation found in a series of experiments performed without catalyst. Although all experiments were carried out in the same way, this effect might not have been exactly the same in all experiments, which may have contributed to the scatter in the results.

3. Results

3.1. Catalyst characterization

The gold content of the catalyst used was determined by ICP-OES, which confirmed the nominal loading of the catalyst amounting to 1.0 wt% Au. The N_2 physisorption showed a catalyst pore volume determined by the BJH method of 0.11 cc g^{-1} and a BET surface area of 49.0 $m^2\,g^{-1}$. The titanium dioxide support has diffraction features characteristic of the Degussa P25 phase consisting of a mixture of anatase and rutile shown in Fig. 2. No diffraction peaks related with the gold crystallites were observed as a result of the low amount of gold in combination with the small average crystallite size that causes a very wide line broadening according to Scherrer's equation.

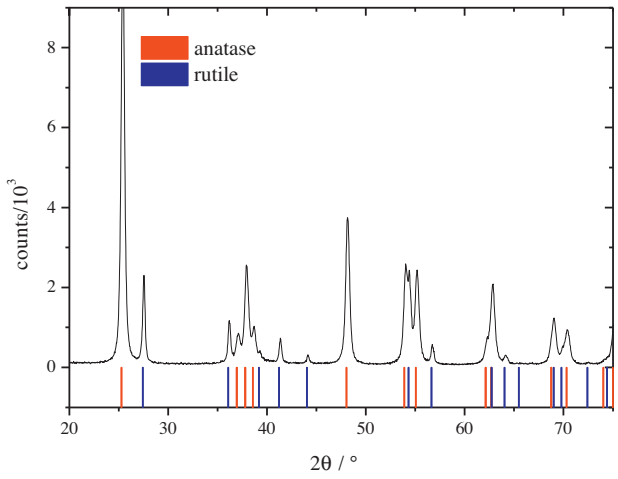

Fig. 2. XRD pattern of the catalyst used.

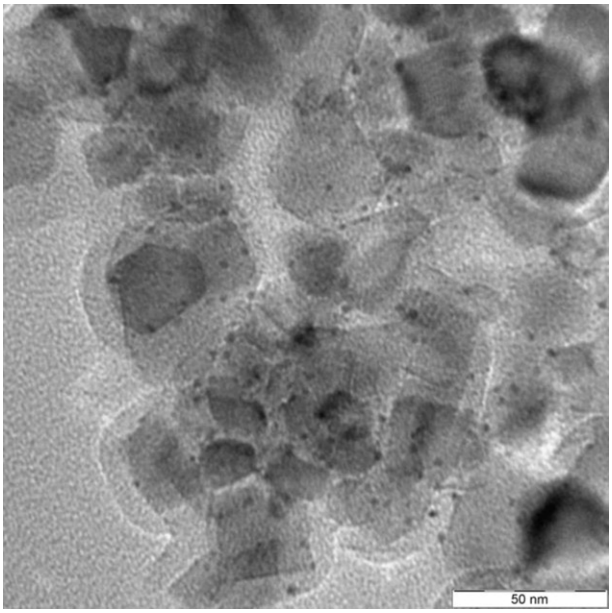

Fig. 3. TEM micrograph of the catalyst used.

TEM images of the catalyst reveal a narrow size distribution of the gold particles deposited on the surface of titanium dioxide. A typical TEM image of the catalyst is shown in Fig. 3. The size distribution of the gold nanoparticles derived, and the result in Fig. 4 shows that almost all crystallites are in the range of 2–6 nm. Statistical analysis of the TEM results yielded an average gold crystallite size of 2.6 nm.

3.2. Kinetic testing

The experimental results of the batch experiments carried out are shown in Fig. 5a-5j together with the results of the optimal fit obtained with the single-site model, which is explained in the following. The symbols are experimental data and the solid lines correspond to the optimal fit. The following abbreviations are used: ethanol (EtOH), acetaldehyde (AcAl), ethyl acetate (EtAc), and acetic acid (AcAc).

Despite some scatter in the data, the results clearly support the reaction sequence of ethanol → acetaldehyde → acetic acid + ethyl acetate, whereas CO_2 is formed at all conditions. Acetaldehyde is a primary reaction product, since it is mainly formed in the beginning; acetic acid is a secondary product, since its selectivity increases with time and catalyst amount. The amount of ethyl acetate initially increases with time, but decreases later indicating that the esterification reaction of acetic acid with ethanol, reaction

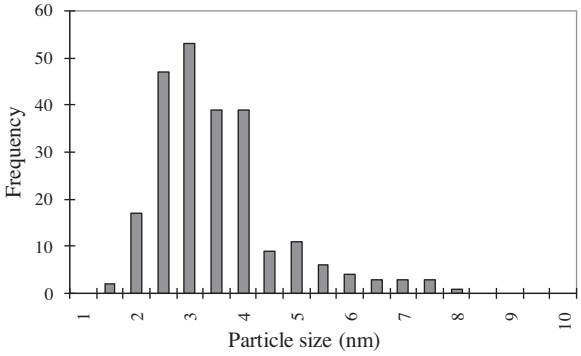

Fig. 4. Au crystallite size distribution of the catalyst used.

4, is close to equilibrium at all times except for the lowest reaction temperatures used. Table 1 contains the reaction scheme that applies to this reaction system.

The results of the experiments, in which the reaction time is varied (Fig. 5a), and the experiments, in which the catalyst concentration is varied (Fig. 5b), yielded similar results and are according to expectation in view of the reaction sequence mentioned above. The results also show that there are no homogeneous reactions, since there was no conversion without catalyst.

The experiments, in which the temperature was varied (Fig. 5c and 5d), show a relatively slow increase of the conversion with increasing temperature, and around 120–130 °C there is even a slight decrease of the conversion. This 'double peak' behavior of Au/TiO_2 in this reaction has already been reported by Simakova et al. [37] for the reaction carried out in the gas phase, for which they found the minimum to be around 160 °C. The authors explained this behavior by two different active reaction species at low and at high temperature [37]. Earlier investigations on the same reaction system in the liquid phase using 1.5 wt% Au on pure anatase TiO_2 [17] and 1 wt% Au on $MgAl_2O_4$ [16], however, did not reveal this 'double-peak' behavior, indicating that it might be related with the reaction medium and/or a rather catalyst-specific behavior.

The experiments, in which the pressure was varied (Fig. 5e-g), show a very weak dependence on the pressure, for the conversion as well as for the selectivities. This very weak pressure dependence was also reported by Christensen et al. [16] on a 1 wt% $Au/MgAl_2O_4$ catalyst.

The results of the experiments, in which the initial ethanol concentration was varied (Fig. 5h-j), show a clear decrease of the conversion with increasing ethanol concentration and also an increase of the acetaldehyde and ethyl acetate selectivity and a decrease of the acetic acid selectivity, particularly at 130 °C and 160 °C, where the ethanol conversion is higher. The changes of the ethyl acetate selectivity and the acetic acid selectivity again show that the composition is close to the esterification equilibrium at these conditions. This tendency was also observed by Christensen et al. [16] on a 1 wt% $Au/MgAl_2O_4$ catalyst.

4. Kinetic modeling and discussion

The reaction scheme in Table 1 has been used for the kinetic modeling. Because Jørgensen et al. [17] observed on Au/TiO_2 that neither aqueous acetaldehyde nor aqueous acetic acid is oxidized to CO_2, reaction 5 of the scheme in Table 1 was eliminated for the kinetic modeling. The authors concluded that the CO_2 production entirely occurs through a non-selective complete oxidation of the reaction intermediate formed directly from adsorbed ethanol, indicated as "CH_3CH_2O".

Since the esterification reaction of acetic acid with the reactant ethanol towards ethyl acetate is very slow without a (e.g. acid) catalyst [38], it is probably a reaction catalyzed by the Au/TiO_2 catalyst as well. The ethyl acetate formation reaction is the only reversible reaction in the reaction scheme, reaching the equilibrium composition if the catalytic activity is high enough.

It is assumed that all reactions occur on the catalyst and that only surface species are involved in the reactions as there is no reaction without catalyst. Probably the oxidation reactions occur on the gold surface, since Jørgensen et al. [17] observed that also $Au/MgAl_2O_4$ is a comparably good catalyst for this reaction, but some interaction with the support cannot be excluded. Since the knowledge about the precise function of the Au and the TiO_2 support and their interaction and also the experimental dataset obtained is insufficient large to allow distinguishing different types of surface sites, only one type of site is assumed for all the oxidation reactions, i.e. competitive adsorption. Fig. 6 illustrates how the first surface reaction step, Reaction 1 in Table 2, might occur. It is assumed that ethanol is activated by H abstraction by a hydroxyl species on the catalyst. Mallat and Baiker [13] also reported that the rate-determining step is probably the cleavage of the C-H bond at the α-carbon atom. However, it cannot be excluded that the H abstraction occurs by an oxygen species and not by a hydroxyl species which also influences the reaction kinetics. The reaction scheme in Table 2 is based on the assumption that hydroxyl species perform the H abstraction.

Since the esterification reaction is specifically catalyzed by acid sites and not by oxidation sites, it is assumed that this reaction occurs on different sites, i.e. non-competitively which might be on the support. The reaction mechanism is accordingly assumed to consist of the set of surface reactions shown in Table 2, in which * stands for a catalytic oxidation site and # stands for an acid catalytic site.

Table 1
Scheme of the oxidation and condensation reactions taking place on the catalyst.

1)	$CH_3CH_2OH + \frac{1}{2}O_2 \rightarrow CH_3CHO + H_2O$
2)	$CH_3CHO + \frac{1}{2}O_2 \rightarrow CH_3COOH$
3)	$CH_3CH_2OH + 3\,O_2 \rightarrow 2CO_2 + 3\,H_2O$
4)	$CH_3COOH + CH_3CH_2OH \rightleftarrows CH_3COOCH_2CH_3 + H_2O$
5)	$CH_3COOH + 2O_2 \rightarrow 2\,CO_2 + 2H_2O$

Table 2
Scheme of the oxidation surface reactions, in which it is assumed that hydroxyl species perform the H abstraction and the esterification surface reactions. The subscript "s" indicates the surface species leading to the selective reaction towards acetaldehyde; the subscript "ns" indicates the surface species leading to the non-selective reaction towards CO_2.

O_2 ads	$O_2 + 2* \rightleftharpoons 2O*$
H_2O ads	$H_2O + * \rightleftharpoons H_2O*$
OH reaction	$H_2O* + O* \rightleftharpoons 2OH*$
EtOH ads	$CH_3CH_2OH + * \rightleftharpoons CH_3CH_2OH*$
AcAl ads	$CH_3CHO + * \rightleftharpoons CH_3CHO*$
AcAc ads	$CH_3COOH + * \rightleftharpoons CH_3COOH*$
CO_2 ads	$CO_2 + * \rightleftharpoons CO_2*$
Reaction 1)	$CH_3CH_2OH* + OH* \longrightarrow [CH_3CHOH*]_s + H_2O*$ $\downarrow \xrightarrow[-H_2O\ fast]{OH*} CH_3CHO*$
Reaction 2)	$CH_3CHO* + OH* \longrightarrow C_3H\ CO* + H_2O*$ $\downarrow \xrightarrow[fast]{OH*} CH_3COOH*$
Reaction 3)	$CH_3CH_2OH* + OH* \longrightarrow [CH_3CHOH*]_{ns} + H_2O*$ $\downarrow \xrightarrow{OH*}_{fast} \ldots \xrightarrow{fast} CO_2*$
AcAc ads#	$CH_3COOH + \# \rightleftharpoons CH_3COOH\#$
EtOH ads#	$CH_3CH_2OH + \# \rightleftharpoons CH_3CH_2OH\#$
EtAc ads#	$CH_3COOCH_2CH_3 + \# \rightleftharpoons CH_3COOCH_2CH_3\#$
H_2O ads#	$H_2O + \# \rightleftharpoons H_2O\#$
Reaction 4)	$CH_3COOH\# + CH_3CH_2OH\# \rightleftharpoons CH_3COOCH_2CH_3\# + H_2O\#$

Table 3
Kinetic rate expressions of the oxidation reactions.

$$r_1 = k_1 C_{EtOH} \sqrt{C_{H_2O}\sqrt{p_{O_2}}}/DEN \quad (3)$$

$$r_2 = k_2 C_{AcAl} \sqrt{C_{H_2O}\sqrt{p_{O_2}}}/DEN \quad (4)$$

$$r_3 = k_3 C_{EtOH} \sqrt{C_{H_2O}\sqrt{p_{O_2}}}/DEN \quad (5)$$

$$with: DEN = \left(1 + \sqrt{K_{O_2}p_{O_2}} + \sqrt{K'_{H_2O}C_{H_2O}\sqrt{p_{O_2}}} + K_{H_2O}C_{H_2O} + \Sigma K_i C_i\right)^2 \quad (6)$$

$$and: \Sigma K_i C_i \equiv K_{EtOH}C_{EtOH} + K_{AcAl}C_{AcAl} + K_{AcAc}C_{AcAc} + K_{CO_2}C_{CO_2}$$

where:
r_i = reaction rate [mol $kg_{cat}^{-1} s^{-1}$]
k_i = reaction rate constant [unit according to equation]
C_i = concentration [mol m^{-3}]
K_i = adsorption constant [unit according to equation]
p_{O2} = partial pressure of O_2 [bar]

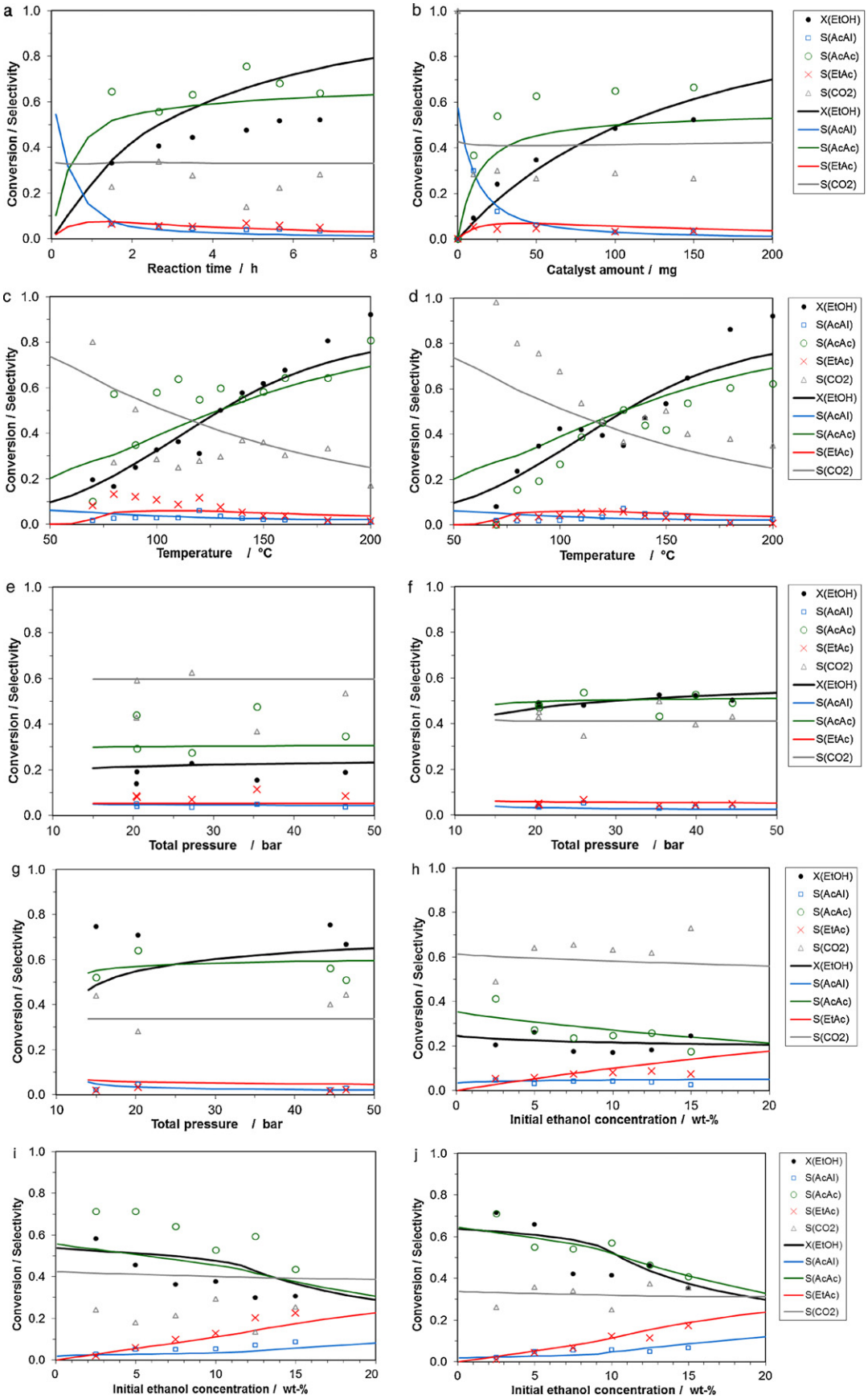

Fig. 5. (a) Reaction time variation at 130 °C. (b) Catalyst concentration variation at 130 °C. (c) Temperature variation (1st experiment). (d) Temperature variation (2nd experiment). (e) Pressure variation at 80 °C. (f) Pressure variation at 130 °C. (g) Pressure variation at 160 °C. (h) Ethanol concentration variation at 80 °C. (i) Ethanol concentration variation at 130 °C. (j) Ethanol concentration variation at 160 °C.

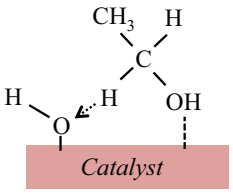

Fig. 6. Schematic drawing of the H abstraction from the adsorbed ethanol molecule, i.e. reaction (1) of the reaction scheme.

These surface reactions can be elaborated to reaction rates involving the corresponding surface species and empty catalytic sites, followed by elimination of the coverages of the surface species. Finally, the reaction rate expressions shown in Table 3 are obtained.

In the term for the denominator, the adsorption constant K'_{H2O} is the adsorption constant resulting from the OH* species, containing a contribution from both H_2O and O_2. Since all experiments were performed using water as solvent, the water concentration has been hardly varied. Correspondingly, the water adsorption constant cannot be estimated from the experimental data. This allows eliminating the water adsorption term, $K_{H2O}C_{H2O}$, from the denominator *DEN*, since this term is constant and can be included in the rate constants. Since the concentrations of acetaldehyde and CO_2 are low at all times, the adsorption terms of these two components were neglected. Since the decrease of the rate at higher initial ethanol concentration increases at higher conversion (i.e. the result at 160 °C compared to that at 80 °C), it is concluded that the adsorption term of acetic acid is much larger than that of ethanol, which leads to the conclusion that also the ethanol adsorption term can be neglected as well. Since the results do not show a negative effect of the pressure on the conversion, the oxygen adsorption term can be neglected comparing to the term involving water and oxygen. This finally reduces the denominator to:

$$DEN = \left(1 + K_{AcAc}C_{AcAc} + \sqrt{K'_{H_2O}C_{H_2O}\sqrt{p_{O_2}}}\right)^2 \quad (7)$$

Since the assumption that the H abstraction occurs by oxygen species instead of by hydroxyl species, as illustrated in Fig. 6, leads to rate expressions with $\sqrt{p_{O2}}$ instead of $\sqrt{(\sqrt{p_{O2}})}$ in the numerator, the kinetic model that follows from this assumption was not further investigated because of the very weak dependence of the conversion on the pressure.

Although the esterification reaction involves surface species as well, probably on acid sites of the catalyst, the kinetic rate expression that follows is the following if it is assumed that the coverages of these acid sites are typically very low:

$$r_4 = k_4 C_{AcAc}C_{EtOH}\left(1 - \frac{C_{EtAc}C_{H_2O}}{K^{eq}_{EtAc}C_{AcAc}C_{EtOH}}\right) \quad (8)$$

Since the experiments were performed in batch operation in a vessel that is assumed to be ideally stirred, the reactor model used to describe the process is the batch reactor model:

$$V_L\frac{dC_{i,L}}{dt} + V_G\frac{dC_{i,G}}{dt} = V_L C_{cat}\sum_j \nu_{i,j}r_j \quad (9)$$

where

V_L = liquid volume in the reactor [m^3]

$C_{i,L}$ = concentration of component *i* in the liquid phase [mol m^{-3}]

t = time [s]

V_G = vapor volume in the reactor [m^3]

$C_{i,G}$ = concentration of component *i* in the vapour phase [mol m^{-3}]

C_{cat} = catalyst concentration [kg m^{-3}]

Table 4
Fractions of the liquid components in the vapor phase based on a liquid volume of 10 mL and a gas volume of 90 mL (vapor pressure equations taken from Yaws 1999 [39]).

Temperature	Ethanol	Acetaldehyde	Acetic acid	Ethyl acetate	Water
150 °C	5%	15%	1.3%	4%	2.6%
200 °C	15%	36%	4%	9%	8%

$\nu_{i,j}$ = stoichiometric coefficient of component *i* in reaction *j* [–]

r_j = reaction rate of reaction *j* [mol kg_{cat}^{-1} s^{-1}]

For O_2 and CO_2 the first term of this equation can be neglected compared to the second term due to their low solubility in aqueous solutions. Using the vapor pressures of the liquid components it appears that particularly at higher temperatures a significant proportion will be present in the vapor phase. Table 4 shows the fraction of the components present in the vapor phase at two different temperatures.

Since it appears that only the lower part of the gas volume reaches the reaction temperature, whereas the upper part is colder due to the vicinity of the colder bare head of the reaction vessel, the actual fractions in the vapor phase were lower than calculated above. Since additionally the evaporation of water results in an increase of the catalyst concentration, which largely compensates the effect of evaporation of the liquid components, the contribution of the vapor phase was for simplicity neglected for all liquid components.

In view of the low concentrations used (5 wt% ethanol in most experiments) it was also assumed that the liquid behaves ideally. Since the liquid significantly expands with increasing temperature, e.g. by 25% at 200 °C, the change of the liquid volume as a function of the temperature has been taken into account. For simplicity, the liquid mixture density mixture was estimated to be the weighted average of the density of pure ethanol and pure water at the reaction temperature, taken from Yaws 2003 [40]. In the simulations, the reactions occurring during the heating time as well as the cooling time were properly taken into account.

The small catalyst particle size range used (10 μm and smaller), in combination with the rather low reaction rate, excluded the occurrence of any mass transport limitation in the catalyst particles. The extent of internal diffusion limitation was estimated using the Weisz-Prater criterion (Froment & Bischoff [41], Anderson & Pratt. [42]), yielding the Wheeler-Weisz modulus,Φ.

$$\Phi = \left(\frac{n+1}{2}\right)\frac{R_v^{obs}\left(d_p/6\right)^2}{D_{eff}\,C_i} \quad (10)$$

Where:

Φ = Wheeler-Weisz modulus [–]

n = reaction order [–]

$R^{obs}_{v,A}$ = observed reaction rate per unit particle volume [mol m^{-3} s^{-1}]

d_p = particle diameter [m]

D_{eff} = effective diffusivity in particle [m^2 s^{-1}]

C_i = concentration [mol m^{-3}]

At the highest temperature used, being 200 °C, the Wheeler-Weisz modulus amounts to 0.0032 for O_2 and 0.00014 for ethanol, which is still far below the limit of 0.08 above which internal diffusion limitation becomes significant. In this calculation, an initial reaction rate of 0.175 mol $kg_{cat}^{-1}s^{-1}$ was used, which corresponds to an ethanol conversion of 97% after 4 hours. The effective diffusivity of oxygen was estimated at 1.3×10^{-9} m^2s^{-1} and for ethanol at 7.8×10^{-10} m^2s^{-1} and the particle size used for the estimation was 10 μm. An oxygen concentration of 12.0 mol m^{-3} was used (i.e. the value at 200 °C), calculated with the correlation from Battino [43]. A check on the external mass transfer limitation, i.e. limitation of

Table 5
Optimal estimates of the kinetic parameters using all experimental data.

Parameter	Unit	Estimate	95% confidence range	
			Value	Relative (%)
k_1 at 130 °C	$[m^{4.5}mol^{-0.5}bar^{-0.25}kg_{cat}^{-1}\ s^{-1}]$	1.320×10^{-5}	$\pm 2.3 \times 10^{-8}$	± 0.17
k_2 at 130 °C	$[m^{4.5}mol^{-0.5}bar^{-0.25}kg_{cat}^{-1}\ s^{-1}]$	4.260×10^{-4}	$\pm 7.2 \times 10^{-7}$	± 0.17
k_3 at 130 °C	$[m^{4.5}mol^{-0.5}bar^{-0.25}kg_{cat}^{-1}\ s^{-1}]$	9.164×10^{-6}	$\pm 2.3 \times 10^{-8}$	± 0.25
E_{a1}	[kJ mol^{-1}]	−2.52	± 0.005	± 0.20
E_{a2}	[kJ mol^{-1}]	−23.17	± 0.05	± 0.22
E_{a3}	[kJ mol^{-1}]	−20.87	± 0.04	± 0.21
K_{AcAc} at 130 °C	[m^3 mol^{-1}]	8.667×10^{-4}	$\pm 1.3 \times 10^{-6}$	± 0.15
K_{H2O} at 130 °C	[m^3 mol^{-1} bar$^{-0.5}$]	5.180×10^{-5}	$\pm 7.9 \times 10^{-8}$	± 0.15
$\Delta H_{ads,AcAc}$	[kJ mol^{-1}]	−71.73	± 0.18	± 0.25
$\Delta H_{ads,H2O}$	[kJ mol^{-1}]	−45.84	± 0.07	± 0.16
k_4 at 130 °C	$[m^6mol^{-1}kg_{cat}^{-1}\ s^{-1}]$	2.505×10^{-5}	$\pm 3.9 \times 10^{-8}$	± 0.16
E_{a4}	[kJ mol^{-1}]	198.8	± 0.27	± 0.13
Objective function	[–]	793	–	–
SSQ*	[–]	529	–	–

*) $SSQ = \sum_{i,k} \left(y_{i,k,exp} - y_{i,k,mod}\right)^2$ (sum of the squared residuals) (y = response, i = component, k = reaction number).

mass transfer from the liquid bulk to the particle, showed that this is also completely negligible.

The dependence of the reaction rate constants on the temperature is assumed to be according to the Arrhenius relationship:

$$k_{j,T} = k_{j,0} \exp\left\{\frac{-E_{aj}}{RT}\right\} \equiv k_{j,T_{ref}} \exp\left\{\frac{-E_{aj}}{R}\left(\frac{1}{T} - \frac{1}{T_{ref}}\right)\right\} \quad (11)$$

where
$k_{j,T}$ = rate constant of reaction j at the actual temperature
$k_{j,0}$ = rate constant of reaction j at infinite temperature
E_{aj} = activation energy of reaction j [J mol^{-1}]
$k_{j,Tref}$ = rate constant of reaction j at the reference temperature
R = ideal gas constant [J mol^{-1} K^{-1}]
T_{ref} = reference temperature, set at 403.15 K (130 °C).

The adsorption constants K_{AcAc} and K_{H2O} in the term *DEN* are also a function of the temperature. If the slight dependence of the adsorption enthalpy and entropy on temperature is ignored, this relationship is (again with T_{ref} = 130 °C):

$$K_{i,T} = K_{i,0} \exp\left\{\frac{-\Delta H_{ads,i}}{RT}\right\} = K_{i,T_{ref}} \exp\left\{\frac{-\Delta H_{ads,i}}{R}\left(\frac{1}{T} - \frac{1}{T_{ref}}\right)\right\} \quad (12)$$

where
$K_{i,T}$=adsorption constant of component i at the actual temperature, T
$K_{i,0}$=adsorption constant of component i at infinite temperature
$\Delta H_{ads,i}$=adsorption enthalpy of component i [J mol^{-1}]
$K_{i,Tref}$=adsorption constant of component i at the reference temperature

The kinetic model contains 14 parameters that are to be estimated using the experimental data: 4 rate constants with 4 activation energies (k_1–k_4) and 2 adsorption constants with 2 adsorption enthalpies (K_{AcAc} and K_{H2O}), and the esterification equilibrium constant and its temperature dependency. This equilibrium constant, $K^{eq}{}_{EtAc}$, and its temperature dependency by means of the reaction enthalpy, ΔH_r, were obtained from the experimental data assuming the experimentally observed compositions to be at equilibrium. Taking the results from all experiments, this relationship was found to be:

$$K^{eq}_{EtAc} = K^{eq}_{EtAc,T_{ref}} \exp\left\{\frac{-\Delta H_r}{R}\left(\frac{1}{T} - \frac{1}{T_{ref}}\right)\right\} \quad (13)$$

where
$K^{eq}_{EtAc,T_{ref}}$ = 4.3 = equilibrium constant at T_{ref} (standard deviation 0.15)
ΔH_r = -8.3 kJ/mol = reaction enthalpy (standard deviation 1.1)

This result corresponds quite well with the value of about 3.7 reported by Cantela and Billinger [43] and the range of 4.0 ± 0.2 at 80 °C reported by Kirbaşlar et al. [44], with a negligible dependence on the temperature in the range of 50–80 °C. The good agreement

Table 6
Correlation matrix between all the parameters estimated with the optimized kinetic model.

	k_1 at 130 °C	k_2 at 130 °C	k_3 at 130 °C	E_{a1}	E_{a2}	E_{a3}	K_{AcAc} at 130 °C	K_{H2O} at 130 °C	$\Delta H_{ads,AcAc}$	$\Delta H_{ads,H2O}$	k_4 at 130 °C	E_{a4}
k_1 at 130 °C	1											
k_2 at 130 °C	−0.18	1										
k_3 at 130 °C	0.11	−0.04	1									
E_{a1}	−0.08	−0.16	−0.19	1								
E_{a2}	−0.42	0.29	0.16	0.14	1							
E_{a3}	0.11	0.13	0.12	−0.08	0.12	1						
K_{AcAc} at 130 °C	−0.11	0.26	0.15	0.09	0.05	0.18	1					
K_{H2O} at 130 °C	0.25	0.00	−0.04	0.02	0.12	−0.06	−0.22	1				
$\Delta H_{ads,AcAc}$	0.31	−0.10	0.32	0.03	−0.39	0.46	0.12	−0.44	1			
$\Delta H_{ads,H2O}$	0.37	−0.60	0.06	0.40	−0.10	0.18	0.00	−0.19	0.24	1		
k_4 at 130 °C	0.14	0.02	0.50	−0.06	0.25	0.17	0.11	0.10	−0.03	0.34	1	
E_{a4}	−0.24	0.37	0.27	−0.10	0.43	0.03	0.01	−0.07	−0.06	−0.08	0.03	1

shows that the experimentally observed values are probably appropriate, and therefore the experimentally determined relationship of the equilibrium constant was used in the simulations in kinetic parameter fitting.

The complete experimental dataset used for the parameter estimation contains 276 experimental data points obtained in 69 batch experiments at various conditions. The parameter estimation was carried out using the software package Athena Visual Studio [45], applying Bayesian estimation for multi-response experiments using a diagonal covariance matrix. As the input for the objective function to be optimized for Bayesian estimation [46], the molar fractions of the four measured liquid components were used. It appeared that the data allowed a proper estimation of all the kinetic parameters involved and the results are shown in Table 5.

From the modeling results, which are included in Fig. 5a-j, it appears that the model is able to adequately describe both conversion and selectivies when taking the scatter into account. The negative influence of the ethanol concentration on the conversion is properly described; it is the result of the combined effect of the inhibiting adsorption term of acetic acid in the denominator DEN and the esterification equilibrium. Only the model predictions for the conversion at the highest temperatures used, 180 °C and 200 °C (Fig. 5c and 5d), and at low pressure at 160 °C (Fig. 5 g) show some deviation which could not be adequately fitted. For the high temperatures this would require an expansion of the model with a second reaction route, which will be briefly discussed at the end of this paper.

The results in Table 5 show that the first three reactions show a negative apparent activation energy. Although negative apparent activation energies are rather unusual, it often occurs when the Langmuir-Hinshelwood-Hougen-Watson type rate equations used since the apparent activation energy of the corresponding rate constants also include the adsorption enthalpies of the adsorbing components implicitly included in the numerator, which are typically negative. For example, in the first reaction the rate constant includes the adsorption energy of ethanol, water, and oxygen. In fact, the rate constant k_1 in Eq. (3) is a lumped parameter, representing the following:

$$k_1 = k_1' K_{EtOH} \sqrt{K_{H_2O} \sqrt{K_{O_2}}}$$

where k_1' is the bare rate constant.

Only for the esterification reaction a high positive activation energy was found, which is well understandable since it was assumed that the final composition of the liquid mixture corresponds to the composition according to the equilibrium constant because the reaction stops very quickly upon cooling down, maintaining the equilibrium composition.

T he correlation matrix for the estimated parameters, available in Table 6, shows that there are no strong correlations between any of the parameters, confirming an accurate estimation.

It is interesting to compare the reaction kinetics with those reported by Jørgensen et al. [17]. Using aqueous ethanol (5 wt%) at 35 bar in air they obtained at 150°C a reaction rate of 2.04×10^{-3} mol kg_{cat}^{-1} s^{-1}. Our kinetic model predicts at these contains exactly twice this rate, despite the lower gold loading (1.5 and 1.0 wt%, respectively). The difference might be related with the size of the gold crystallites, the support, or some deactivation.

4.1. Two-sites model

Finally, it was attempted to improve the model by introducing a second active site, or a second reaction route (and using the same shape of the rate equations), in order to get a better description of the temperature variation experiments. Although this indeed enables to describe some kind of a dip in the activity around 130 °C and also the high conversion at 180 and 200 °C, the kinetic model contains too many parameters, i.e. 20, to achieve a statistically justifiable model. Fitting such a model requires many more experimental data or data with less scatter.

5. Conclusions

The commercial 1 wt% Au/TiO_2 catalyst used in this study, containing gold crystallites of around 2.6 nm, showed a high activity for the selective oxidation of aqueous ethanol to mainly acetic acid. This catalytic system utilizes air as clean oxidant and it seems interesting for large-scale application due to its simplicity of operation and environmentally friendliness since it does not generate harmful by-products. By variation of the reaction conditions, i.e. temperature, pressure, initial ethanol concentration, catalyst concentration, and reaction time, a set of experimental data was obtained which was fitted adequately into a Langmuir–Hinshelwood–Hougen–Watson kinetic model based on catalytic surface reactions. Hydrogen abstraction by surface hydroxyl species was assumed to be the rate-determining step. A two-sites model, or a second reaction mechanism, might be developed with additional experimental data to achieve a better description of the slight dip in conversion around 130 °C and the rapid increase of the conversion at 180 and 200 °C.

Acknowledgements

We are pleased to acknowledge generous support for this work by Laboratory of Industrial Chemistry at Ruhr University of Bochum. The authors thank Professor Martin Muhler in particular for the opportunity to perform the experiments.

References

[1] R.A. Sheldon, J.K. Kochi, Metal-Catalyzed Oxidations of Organic Compounds, Academic Press, New York, 1981.
[2] D.I. Enache, J.K. Edwards, P. Landon, B. Solsona-Espriu, A.F. Carley, A.A. Herzing, M. Watanabe, C.J. Kiely, J.D.W. Knight, G.J. Hutchings, Science 311 (2006) 362.
[3] M. Vazylyev, D. Sloboda-Rozner, A. Haimov, G. Maayan, R. Neumann, Topics in Catalysis 34 (2005) 93.
[4] M. Pagliaro, S. Campestrini, R. Ciriminna, Chemical Society Reviews 34 (2005) 837.
[5] K. Mori, T. Hara, T. Mizugaki, K. Ebitani, K. Kaneda, Journal of the American Chemical Society 26 (2004) 10657.
[6] I.E. Marko, P.R. Giles, M. Tsukazaki, S.M. Brown, C.J. Urch, Science 274 (1996) 2044.
[7] G. Cainelli, G. Cardillo, Chromium Oxidations in Organic Chemistry, Springer-Verlag, Berlin, 1984.
[8] W.P. Griffith, J.M. Joliffe, Studies in Surface Science and Catalysis 66 (1991) 395.
[9] D.G. Lee, U.A. Spitzer, Journal of Organic Chemistry 35 (1970) 3589.
[10] R.A. Sheldon, I.W.C.E. Arends, A. Dijksman, Catalysis Today 57 (2000) 157.
[11] R.A. Sheldon, I.W.C.E. Arends, G.J. Brink, A. Dijksman, Accounts of Chemical Research 35 (2002) 774.
[12] M. Besson, P. Gallezot, Catalysis Today 57 (2000) 127.
[13] T. Mallat, A. Baiker, Chemical Reviews 104 (2004) 3037.
[14] W. Hou, N.A. Dehm, R.W.J. Scott, Journal of Catalysis 253 (2008) 22.
[15] A. Abad, P. Concepcion, A. Corma, H. Garcia, Angewandte Chemie International Edition 44 (2005) 4066.
[16] C.H. Christensen, B. Jørgensen, J.R. Hansen, K. Egeblad, R. Madsen, S.K. Klitgaard, S.M. Hansen, M. Rass-Hansen, H.C. Andersen, A. Riisager, Angewandte Chemie International Edition 45 (2006) 4648.
[17] B. Jørgensen, S.E. Christiansen, M.L.D. Thomsen, C.H. Christensen, Journal of Catalysis 251 (2007) 332.
[18] D.I. Enache, D.W. Knight, G.J. Hutchings, Catalysis Letters 103 (2005) 43.
[19] D.I. Enache, D. Barker, J.K. Edwards, S.H. Taylor, D.W. Knight, A.F. Carley, G.J. Hutchings, Catalysis Today 122 (2007) 407.
[20] J. Schwank, Gold Bulletin 16 (1983) 103.
[21] G.C. Bond, D.T. Thompson, Catalysis Reviews Science and Engineering 41 (1999) 319.
[22] M. Haruta, Chemical Record 3 (2003) 75.
[23] M. Haruta, N. Yamada, T. Kobayashi, S. Iijima, Journal of Catalysis 115 (1989) 301.
[24] M. Kotobuki, R. Leppelt, D.A. Hansgen, D. Widmann, R.J. Behm, Journal of Catalysis 264 (2009) 67.

[25] R.M. Finch, N.A. Hodge, G.J. Hutchings, A. Meagher, Q. Pankhurst, M.R.H. Siddiqui, F.E. Wagner, R. Whyman, Physical Chemistry Chemical Physics 1 (1999) 485.
[26] C.K. Costello, M.C. Kung, H.-S. Oh, Y. Wang, H.H. Kung, Applied Catalysis A 232 (2002) 159.
[27] M.C. Kung, R.J. Davis, H.H. Kung, Journal of Physical Chemistry C 111 (2007) 11767.
[28] N. Lopez, T.V.W. Janssens, B.S. Clausen, Y. Xu, M. Mavrikakis, T. Bligaard, J.K. Nørskov, Journal of Catalysis 223 (2004) 232.
[29] N. Lopez, J.K. Nørskov, T.V.W. Janssens, A. Carlsson, A. Puig-Molina, B.S. Clausen, J.D. Grunwaldt, Journal of Catalysis 225 (2004) 86.
[30] M. Mavrikakis, P. Stoltze, J.K. Nørskov, Catalysis Letters 64 (2000) 101.
[31] C.K. Costello, M.C. Kung, H.-S. Oh, Y. Wang, H.H. Kung, Applied Catalysis A 232 (2002) 159.
[32] S.H. Overbury, V. Schwartz, D.R. Mullins, W. Yan, S. Dai, Journal of Catalysis 241 (2006) 56.
[33] M. Haruta, Catalysis Surveys From Japan 1 (1997) 61.
[34] M.M. Schubert, S. Hackenberg, A.C. van Veen, M. Muhler, V. Plzak, R.J. Behm, Journal of Catalysis 197 (2001) 113.
[35] L.M. Molina, M.D. Rasmussen, B. Hammer, Journal of Chemical Physics 120 (2004) 7673.
[36] www.strem.com and http://www.mintek.co.za
[37] O.A. Simakova, V.I. Sobolev, K.Yu. Koltunov, B. Campo, A.-R. Leino, K. Kordás, D.Yu. Murzin, ChemCatChem 2 (2010) 1535.
[38] R.C. Cantela, R.D. Billinger, Journal of the American Chemical Society 50 (1928) 3212.
[39] C.L. Yaws, Chemical Properties Handbook, McGraw-Hill, Inc., New York, 1999.
[40] C.L. Yaws, Yaws' Handbook of Thermodynamic and Physical Properties of Chemical Compounds, Knovel, 2003.
[41] G.F. Froment, K. Bischoff, Chemical Reactor Analysis and Design, J. Wiley & Sons, New York, 1990.
[42] J.R. Anderson, K.C. Pratt, Introduction to Characterization and Testing of Catalysts, Academic Press, Sydney, 1985.
[43] R. Battino, Solubility data series, Oxygen and ozone, in: A.S. Kertes (Ed.), vol. 7, IUPAC, Pergamon Press, Oxford, 1981.
[44] Ş.I. Kirbaşlar, S.B. Baykal, U. Dramur, Turkish Journal of Engineering and Environmental Sciences 25 (2001) 569.
[45] Athena Visual Studio, Software for modeling, estimation and optimization, Version 12.1 (www.AthenaVisual.com), 1997–2009.
[46] W.E. Stewart, M. Caracotsios, J.P. Sørensen, AIChE Journal 38 (1995) 641.